7656 *Biochemistry* **2009,** *48,* 7656–7664
DOI: 10.1021/bi900626u

BIOCHEMISTRY
including biophysical chemistry & molecular biology
Article

Amyloid Fibrillation of Human Apaf-1 CARD[†]

P. Nageswara Rao, K. Sony Reddy, and Abani K. Bhuyan*

School of Chemistry, University of Hyderabad, Hyderabad 500046, India

Received April 11, 2009; Revised Manuscript Received July 13, 2009

ABSTRACT: The idea of establishing the amyloid-like fibrillation tendency of pro- and antisurvival proteins of human apoptotic pathways is relevant for delineating the conditions that lead to aberrant differentiation, development, and tissue homeostasis. As the first step in this direction, we report here that the caspase recruitment domain (CARD) of recombinant human apoptotic protease activating factor-1 (Apaf-1) can be induced to undergo amyloid-like fibrillation. The study was initiated with a set of biophysical investigations into the possibility and in vitro conditions for fibril growth. By scanning the pH-induced conformational transitions, protein stability, and stopped-flow folding−unfolding kinetics, we detected a molten globule (MG) transition of the CARD at pH < 4. In a bid to reduce the surface-accessible hydrophobic patches in the MG state, the CARD monomer undergoes self-association to produce soluble oligomers that serve as precursor aggregates for protofibril formation. The monomer-to-oligomer self-association process is akin to the well-known homophilic CARD−CARD interaction by which CARDs of the same or different apoptotic proteins associate to transduce and regulate the apoptotic signal. The fibrillation reaction of the Apaf-1 CARD was conducted at pH 2.1 and 60 °C, because reduction of exposed hydrophobic surfaces in the MG state is more favored under the moderated solution condition. The Gaussian distributions of diameters of the fibril population suggest values of 2.1 and 2.7 nm for the mean diameter of precursor aggregates and protofibrils or elongated fibrils, respectively.

The supramolecular assembly of a sizable number of diverse proteins and polypeptides into amyloid and amyloid-like fibrils has attracted the attention of many for a number of reasons. First, the pathogenesis of a number of human conditions, including Alzheimer's disease, Parkinson's disease, spongiform encephalopathy, Huntington's disease, senile amyloidosis, and type II diabetes (*1*−*7*), is fundamentally associated with amyloids. A detailed understanding of the processes leading to extracellular amyloid deposition, intracellular neurofibrillary tangles, and the development of amyloid toxicity is necessary in devising strategies for therapeutic intervention and management of these diseases. Such β-sheet-based structural assemblies are also promising for industrial application, and in material science and biotechnology (*21*−*26*). Second, the observation that a wide variety of non-disease-related proteins and polypeptides that presumably do not undergo amyloid-like transitions in vivo but can be induced to do so in test tubes via a change in the solution conditions (*5*, *8*−*13*) has added newer dimensions to the multifarious response of proteins to solvent conditions. Given the number and variety of proteins from which amyloids have been formed, it is now generally accepted that amyloid aggregates are a generic structure for all proteins (*14*). Since the amino acid composition, sequence, and native-state structure are not determinants of amyloidogenecity (*2*, *14*), amyloid fibrillation could originate from anywhere in the conformational landscape, entropically as low as the native or nativelike states to as high as unfolded states in a protein-specific manner (*2*, *15*, *16*), implying that some combination of the initial structure, number of intramolecular contacts, chain dynamics, and surface dielectric may be required to promote fibrillation and that these factors may also be related to the kinetic mechanism of the composite fibrillation reaction. Our understanding of such issues needs to be augmented. Atomic models of amyloid fibril structure based on various pieces of evidence, each limited by the extent amenable to the experiment, have been discussed (*17*−*20*). Although there is a consensus that amyloid and amyloid-like fibrils contain β-sheet conformations, achieving atom-level resolution of arrangements of β-sheet structures has been seriously hindered by the difficulties of handling fibrous supramolecular forms that are often insoluble, especially at concentrations required for structural work. Thus, the specific structural and chemical features of proteins and the solvent-dependent reactivity that promote amyloidogenesis are at the focus of current research.

With regard to the etiology of amyloid cytotoxicity at the molecular level, fewer studies conducted to date have indicated that the fibrils and the precursor β-oligomers trigger apoptosis in cells (*27*−*35*). These in vitro studies confined to cultured neurons have relied principally on the observation of cell morphology and biochemical characteristics of apoptosis in response to treatment with soluble fibrils and precursor aggregates (PA).[1] The evidence that amyloid-induced activation of an apoptotic pathway is one of the reasons for neural cell death in neurodegenerative diseases is compelling.

[†]This work was supported by a grant (4/1/2003-SF) from the Department of Science and Technology, Government of India.

*To whom correspondence should be addressed. E-mail: akbsc@uohyd.ernet.in. Phone: 91-40-2313-4810. Fax: 91-40-2301-2460.

[1]Abbreviations: Apaf-1, apoptotic protease activating factor-1; CARD, caspase recruitment domain; PA, precursor aggregate; GST, glutathione *S*-transferase; MG, molten globule; ANS, 8-anilinonaphthalene-1-sulfonate; GdnHCl, guanidine hydrochloride; $\Delta G°$, Gibbs energy of denaturation in the absence of denaturant; AFM, atomic force microscopy; fwhm, full width at half-maximum; PDB, Protein Data Bank.

 Published on Web 07/15/2009

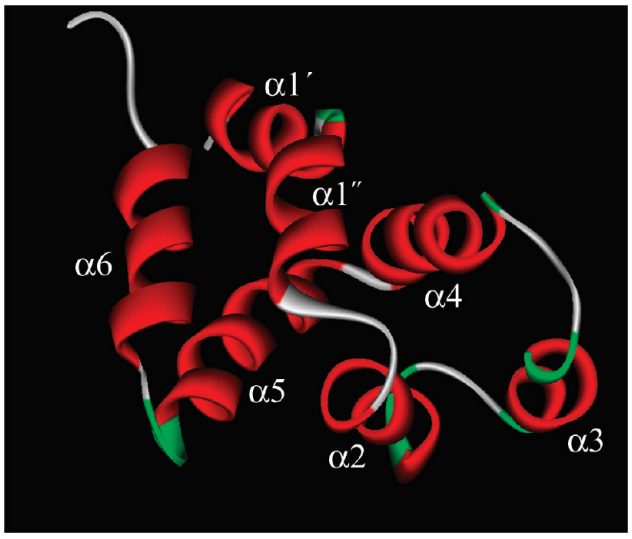

FIGURE 1: Ribbon diagram of the Apaf-1 CARD (PDB entry 1C15) with helices labeled (*38*).

We were contemplating the general possibility of an amyloid-like transition of the pro- and antisurvival proteins of mammalian apoptotic pathways, even though at present there is no known amyloidosis that results from aggregation of any of these proteins, wild-type or otherwise. Should any of them undergo amyloid fibrillation, the normal development, tissue differentiation, and homeostasis will be critically affected. To touch upon this possibility, this study reports on the in vitro transformation of the recombinant CARD of human Apaf-1 (Figure 1) into amyloid protofibrils. Apaf-1, a large antisurvival protein (~130 kDa), is the key molecule for activation of procaspase-9 in the mitochondrial pathway of apoptosis in neuronal and somatic cells alike (*36*, *37*). Structurally, the Apaf-1 CARD consists of six tightly packed amphipathic α-helices [Figure 1 (*38*)]. The CARD is used because this domain is present as the N-terminal prodomain in a sizable set of apoptotic proteins, including some caspases, and CARDs are known to mediate apoptotic signaling through homophilic CARD−CARD interactions (*38*−*42*). To arrive at the in vitro conditions for transformation of the CARD protein to fibrils, we conducted a series of biophysical experiments as the prelude. The results of pH-dependent conformational transitions, protein stability, and folding−unfolding kinetics showed that the Apaf-1 CARD undergoes a MG-like transition under acidic conditions. This low-pH-denatured form of the CARD then undergoes further conformational transitions to produce soluble PA of amyloid-like protofibrils.

MATERIALS AND METHODS

Cloning and Generation of the CARD Expression Construct. Total RNA isolated from HeLa cells was used for the cDNA amplification of the 300 bp gene fragment of Apaf-1. Forward and reverse CARD primers were designed with pGEX4T-1 compatible restriction sites at their 5′ ends. The forward primer has a BamHI site and the reverse a XhoI site: CARD-F, 5′ CGGGATCCATGGATGCAAAAGCTCGAA 3′ (BamHI site underlined); CARD-R, 5′ CCCTCGAGCTAAGAAGAGACAACAGGAATG 3′ (XhoI site underlined). The cDNA was synthesized by reverse transcriptase, and the 300 bp CARD fragment was amplified by Taq DNA polymerase. Both steps were achieved by using the "one-step RT-PCR kit" from ABGene Technologies. The PCR-amplified fragment was isolated by the standard procedure, ligated into the TA cloning vector, and transformed into DH5α bacterial cells by the standard $CaCl_2$ procedure. The transformed cells were plated onto LB agar plates with 100 μg/mL ampicillin and 1 mM IPTG. The positive clones, selected by blue-white screening and colony PCR, were used for isolation of plasmid DNA by standard protocols.

The PCR fragment cloned into the TA cloning vector was restricted using BamHI and XhoI and analyzed on a 1% agarose gel. The pGEX4T-1 expression vector was also restricted in the same manner. The CARD gene fragment was then ligated into digested pGEX4T-1 by using T4 DNA ligase and transformed into DH5α cells. Cell colonies positive with the recombinant plasmid were screened by colony PCR. That the recombinant plasmids contained the expression vector carrying the insert was once again checked by restriction digestion. The sequence and orientation of the CARD fragment were confirmed by sequencing. The restriction-positive plasmids were transformed into *Escherichia coli* BL21 cells for expression of the CARD protein.

Protein Expression and Purification. LB broth (500 mL) with 100 μg/mL ampicillin was inoculated with 25 mL of a culture grown overnight (1:20 ratio) that contained the recombinant positive clone. Protein expression was induced at an OD_{600} of 0.5 with 1 mM IPTG. Cells were grown for 5 h at 37 °C. Cells were pelleted, resuspended in 20 mL of PBS, and lysed by sonication for 3 min with repetitive 30 s on and off cycles. The lysate was centrifuged at 3000*g* for 30 min at 4 °C. The supernatant was collected, and DTT was added to a final concentration of 1 mM. This was loaded onto a 1 mL GSH Sepharose 4B column that was preequilibrated with 10 volumes of PBS. The column was washed with 20 volumes of PBS. The GST−CARD protein that was bound to the column was eluted with 10 volumes of elution buffer [50 mM Tris-HCl and 10 mM reduced glutathione (pH 8)]. The purified GST−CARD protein was dialyzed against 1× PBS to remove the glutathione and digested with recombinant thrombin (Amersham Biosciences) by standard protocols. Following digestion, thrombin was removed by benzamidine Sepharose, and the protein mixture was loaded onto a GSH-Sepharose 4B column. The 10 kDa CARD protein was eluted in the flow-through and was purified further by Sephadex G-75 chromatography.

Equilibrium Measurement of CARD Stability toward pH, NaCl, and GdnHCl. For these titrations, separate samples with identical protein concentrations (5−7 μM) were employed. Protein solutions held at different values of pH or NaCl concentration were incubated for ~6 h before fluorescence spectra were recorded. For GdnHCl unfolding, samples containing different concentrations of the denaturant were prepared by mixing two stock protein solutions, one with 4 M GdnHCl and the other without. Buffers for various pH ranges were as follows: 50 mM glycine for pH < 3, 50 mM sodium acetate for pH 3−5, HEPES, PIPES, and Tris (17 mM each) for pH 6−9, and glycine and CAPS (25 mM each) for pH 9−11. All experiments were conducted at 22 °C using a Fluoromax-4 (Horiba Jobin Yvon) instrument.

Stopped-Flow Kinetics of CARD Folding and Unfolding. These experiments involved two-syringe mixing and invariably employed 8-fold dilution of a 10 μM protein solution with the relevant buffer. For refolding, the protein initially unfolded in 5.4 M GdnHCl and after equilibration for ~1 h was mixed with the refolding buffer containing a variable amount of GdnHCl. Unfolding was initiated by diluting the native protein solution with the unfolding buffer containing desired concentrations of

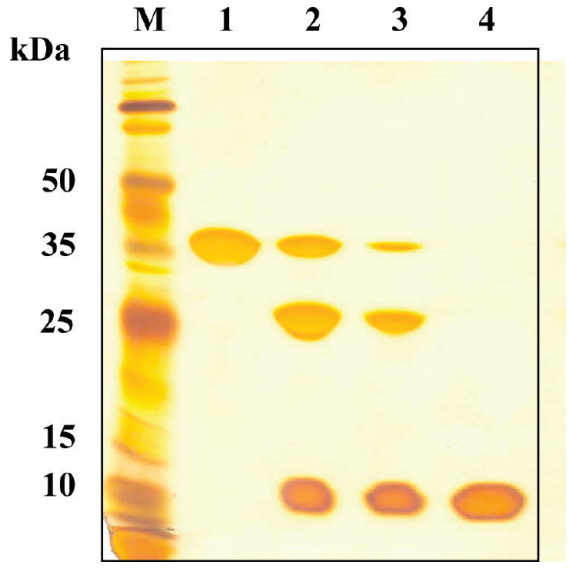

FIGURE 2: Silver-stained SDS−PAGE analysis of purification of the Apaf-1 CARD: lane M, molecular mass markers; lane 1, GST−CARD protein purified from the cell lysate by using a GSH Sepharose 4B column; lane 2, thrombin-digested GST−CARD mixture; lane 3, digest after removal of thrombin by benzidene Sepharose; and lane 4, homogeneous and pure CARD obtained after he thrombin-stripped digest had been passed through a GSH-Sepharose 4B column. The CARD protein elutes in the flow-through fractions.

GdnHCl. The buffer systems were the same as those given above. Kinetics were recorded at 22 °C in a Bio-Logic SFM4 mixing module using a 0.8 mm square flow cell (mixing dead time of ~2 ms). Typically, 8−10 shots were averaged for noise reduction.

Fibrillation Kinetics. CARD solutions (~15 μM) containing ~50 μM thioflavin [4-(3,6-dimethylbenzothiazol-2-yl)-*N*,*N*-dimethylaniline (ThT)] were prepared in 50 mM glycine-HCl buffer (pH 2.1) and incubated at 60 °C in a heating block. Samples incubated for different periods of time were cooled and analyzed by 482 nm ThT fluorescence (excitation at 432 nm) using a Fluoromax-4 (Horiba Jobin Yvon) instrument.

Atomic Force Microscopy. For microscopy, fibrillation was allowed in the absence of thioflavin. Films of samples incubated for variable periods of time were deposited on freshly cleaved mica plates and allowed to dry under nitrogen for ~15 min. We then thoroughly washed the films by gently passing deionized water over the mica plate and dried them under nitrogen for ~1 h. Imaging in the semicontact mode was performed in a NT-MDT Solver microscope using a 3 μm scanner head. Images were processed using the NOVA software supplied by the microscope's manufacturer.

RESULTS

Apaf-1 CARD Expression System and Recombinant Protein. Initially, we generated two gene constructs for *E. coli* expression of the human Apaf-1 CARD, one with an N-terminal His_6 tag (pET28a vector) and the other with GST fused at the N-terminus (pGEX4T-1 vector), but the latter was chosen for the production of the recombinant protein because of the ease and convenience of purifying GST-fused small proteins. This expression vector was used in earlier studies of the NMR solution structure of the Apaf-1 CARD (*38*), although mutagenesis-based cloning and expression in the pET-3d vector have also been reported (*43*). As Figure 2 shows, the recovered CARD (~6 mg/L of *E. coli* culture) is homogeneous and highly pure. Sephadex

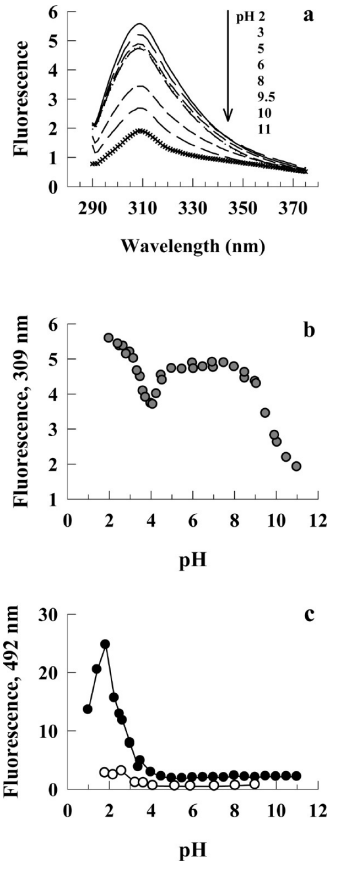

FIGURE 3: Fluorescence-monitored pH dependence of CARD conformational transitions. For all these experiments, the protein concentration was ~6 μM. (a) Fluorescence spectra as a function of pH generally convey enhanced quenching with pH increments. (b) The plot of 309 nm fluorescence with pH, however, shows three prominent transitions: an alkaline transition, a weakly acidic transition, and a more acidic transition. The interpretations and assignment of each of the transitions to specific conformational changes of the CARD are described in the text. Because of the complexity of the analysis of the three linked transitions, the data have not been fitted to a function. (c) Effects of pH on ANS binding to the CARD. The protein and ANS concentrations in the solution at different pHs were 7 and 15 μM, respectively. The empty circles show the 492 nm fluorescence of control samples from which the protein was excluded.

G-75 chromatography consistently show that the purified CARD is monomeric.

Different pH Forms of the CARD. The rationale for examining CARD conformational changes as a function of pH was that partly denatured proteins at acidic and alkaline pH can often reveal structural and functional regulation of proteins. A contextual example is low-pH dimerization of members of the apoptotic Bcl-2 family of proteins which possibly leads to ion channel formation in synthetic membranes (*44*). For the Apaf-1 CARD, Figure 3a shows the general trend of fluorescence decrease with an increasing pH. The primary structure of the CARD has no tryptophan, and the observed fluorescence with a λ_{max} of 309 nm, likely due to tyrosine, is weak. The absence of any shift in the fluorescence maximum across the pH range may be due to the very similar polarity of the environment of tyrosines under native and denaturing conditions. Closer examination of the pH dependence of the 309 nm fluorescence (Figure 3b) shows a pronounced dip at pH ~4 on either side of which the fluorescence signal increases. In the pH range of 5−8, the fluorescence remains unchanged but decreases gradually for pH > 8. The data thus indicate three pH-induced transitions: an alkaline

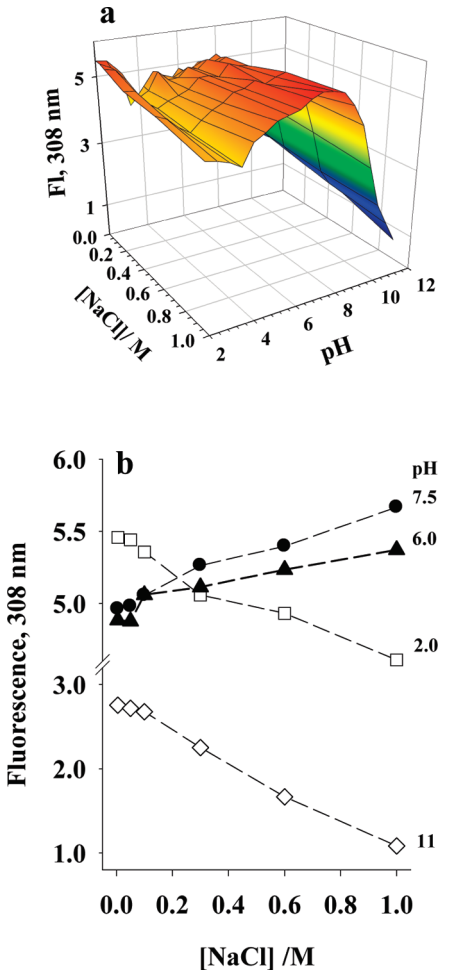

FIGURE 4: CARD fluorescence as a function of pH at different concentrations of NaCl. (a) All three pH-induced conformational transitions of CARD are seen in a NaCl-independent manner, although some details of the transitions, including the sharpness and fluorescence amplitudes, are affected (see Results). (b) The effect of NaCl on the fluorescence amplitude depends on the pH of the medium. The substantial decrease in fluorescence at acidic and alkaline pH is likely due to electrostatic screening of protein charges by Cl^- and Na^+ ions, respectively.

transition with a pH midpoint near 10 attributable to tyrosyl side chain ionization, a weakly acidic transition with a midpoint around pH 4.5 due likely to the ionization of the side chain COOH group of Glu or Asp, and a MG-like transition under moderately strong acidic conditions. While the MG-like transition involves a global denaturation transition of the CARD, the other two transitions could simply be associated with side chain ionization-linked conformational perturbation. As a simple test of the extent of structure perturbation in each of these transitions, we measured the ANS fluorescence of CARD solutions containing ANS (6 μM protein and 12 μM ANS) as a function of pH. As Figure 3c shows, ANS is fluorescence-silent at pH >4 but is very highly fluorescent at pH <4. The ANS fluorescence indicates a major transition in the pH range of 2−4, closely reproducing the MG-like transition considered above (Figure 3b). Indeed, ANS binds to solvent-exposed clusters of hydrophobic groups, and its strong binding is a particularly convenient test for the molten globule state (*45*). However, the ANS fluorescence decreases when the pH value falls below 2 (Figure 3c), indicating self-association or oligomerization of the acid-denatured CARD in a manner that conceals the exposed hydrophobic surfaces. The CARD monomers possibly oligomerize by hydrophobic interactions. Now, the shortage of hydrohphobic surface results in fewer ANS molecules bound, and hence a decrease in fluorescence.

To improve our understanding of the CARD conformational changes further, we extended the pH-dependent fluorescence experiment by including the NaCl concentration as another variable (Figure 4a). Clearly, all three transitions seen in Figure 3b, the alkaline, the acidic, and the MG-like transitions, are reproduced in the presence of any concentration of NaCl used in range of 0−1 M (Figure 4a). In addition, NaCl sets the fluorescence amplitude in a pH-dependent manner (Figure 4b). At intermediate pH values, the fluorescence slightly increases with NaCl but decreases prominently at acidic and alkaline values most likely due to electrostatic screening of protein charges by Cl^- and Na^+ ions, respectively. It means that the added Cl^- and Na^+ ions render the acid or alkali-denatured expanded conformations compact by weakening the electrostatic charge−charge repulsion in the molten globule state (*45*), and a transition from the expanded to compact molecular conformation is expected to decrease the fluorescence intensity (see below). Thus, at pH ~2, the acid-denatured state is transformed to a molten globule state. In summary, the CARD at acidic pH (<4) undergoes a major denaturational transition accompanied by a substantial exposure of otherwise buried hydrophobic surfaces. Under strongly acidic conditions (pH <2), the denatured monomers interact with each other possibly by hydrophobic interactions to produce soluble oligomers or aggregates. We have called them precursor aggregates (PAs).

Equilibrium and Kinetic Aspects of Folding of the Apaf-1 CARD at Acidic and Neutral pH. To learn more about the influence of pH on the stability and structure, we examined the GdnHCl-induced folding behavior of the protein by equilibrium and stopped-flow kinetic methods. Figure 5a shows the equilibrium unfolding transition at pH 6 and 3.1. At pH 6, the initial increase of fluorescence in the pretransition region is followed by a relatively sharp drop in the unfolding transition region. The structural details associated with these changes are subject to scrutiny. For now though, a fit of the data to the two-state $N \rightleftharpoons U$ model (*46*), where N and U are native and unfolded states, respectively, by assuming a second-order polynomial dependence of the pretransition fluorescence with GdnHCl yields the protein stability ($\Delta G^\circ = 12.5 \pm 0.5$ kcal/mol) and the transition midpoint ($C_m \approx 2.4 \pm 0.1$ M). In an earlier study of CARD unfolding in the presence of urea, a value of ~6 kcal/mol was reported for ΔG° (*47*). Generally, the ΔG° value determined by urea unfolding is considerably lower than that extracted from GdnHCl unfolding. Part of the discrepancy also arises from the large increase in the fluorescence in the pretransition baseline (Figure 5a) which the earlier authors did not notice in their study using urea (*47*). At pH 3.1, a clear unfolding transition of the CARD is not detected. The change in the fluorescence stretches out for >1.5 M GdnHCl, indicating less compactness and the lack of well-defined structural elements typical of an acid-denatured state in the absence of added anions (*45*). The monotony of the fluorescence change might simply reflect expansion of the chain. To show that the unfolded state in the presence of 4 M GdnHCl does not contain any considerable structure, the protein was titrated in the pH range of 1−7.5, holding the denaturant concentration constant at 4 M (Figure 5b). Within the error limit, the fluorescence hardly changes in the pH range of 2−7.5, suggesting that unfolding is complete at 4 M GdnHCl.

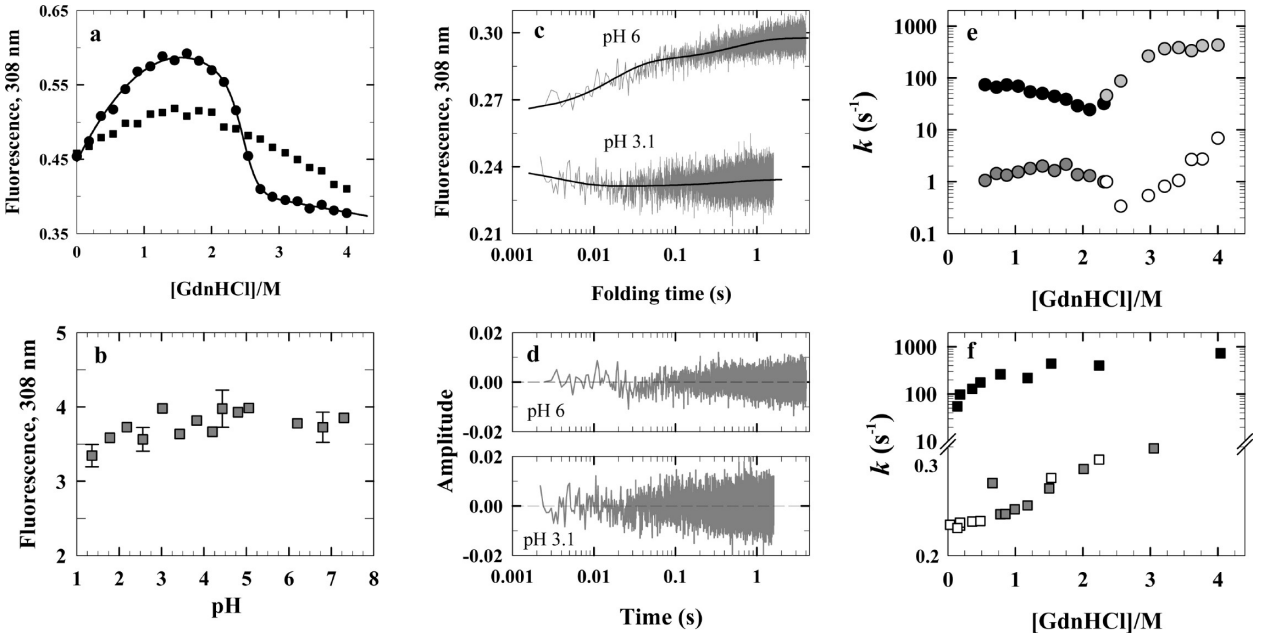

FIGURE 5: pH-dependent stability and folding kinetics of the Apaf-1 CARD. (a) GdnHCl-induced equilibrium unfolding at pH 6 (●) and 3.1 (■). At pH 6, the global unfolding transition is preceded by a pretransition zone characterized by a substantial increase in fluorescence. Since the details of CARD structural changes that occur in the pretransition region are unclear at the moment, the data were modeled with a two-state N ⇌ U transition by assuming that the pretransition changes are due to solvent-dependent baseline effects having a second-order polynomial dependence for fluorescence changes with GdnHCl. The fit of the data yields a $\Delta G°$ of 12.5 ± 0.5 kcal/mol and a C_m of ≈2.4 ± 0.1 M (see the text). At pH 3.1, no pronounced global transition is apparent, suggesting the absence of well-defined tertiary structure. (b) pH titration of the 4 M GdnHCl-unfolded protein. (c) Representative kinetic traces for refolding of the CARD in the presence of 1 M GdnHCl (pH 6) or 0.7 M GdnHCl (pH 3.1). For both experiments, the protein was initially unfolded in 5.4 M GdnHCl at the respective pH. The refolding at pH 6 is described by two rising exponentials: k_{fast} = 60 s^{-1} and k_{slow} = 1.8 s^{-1} with fractional observed amplitudes of 0.7 and 0.3, respectively. At pH 3.1, there is a fast decaying phase (k_{fast} = 262 s^{-1}) followed by a slow rising phase (k_{slow} = 2 s^{-1}), suggesting the possible formation of an aggregate or misfolded intermediate at early times of refolding. (d) Residuals of the two-exponential fits. (e) GdnHCl dependence of the apparent rates for the major phase (top chevron) and the minor phase (bottom chevron) at pH 6. In each chevron, the data forming the left (darker symbols) and right (lighter symbols) arms represent refolding and unfolding, respectively. The rate rollover in the folding arm of each chevron is classically taken as one of the indicators of the presence of folding intermediates. (f) At pH 3.1, the GdnHCl dependence of the apparent rate for the fast kinetic phase (■) shows an unfolding event the rate of which rolls over at > 1 M GdnHCl. This phase may arise from protein aggregation or misfolding. The slow phase (bottom chevron) also barely shows protein refolding at this pH, suggesting the absence of well-defined tertiary structure and packing.

Figure 5c shows two representative kinetic traces for refolding of the CARD, one at pH 6 and the other at pH 3.1, both initially unfolded in 5.4 M GdnHCl at the respective pH and refolded in the presence of 1 M GdnHCl for pH 6, and 0.7 M GdnHCl for pH 3.1. Both traces are best fit by two exponentials, and the residuals are shown in Figure 5d. At pH 6, the two kinetic phases have the same sign for amplitudes and are associated with refolding. At pH 3.1, only the slow rising phase is indicative of refolding. The initial phase which is faster than the slow phase by at least 2 orders of magnitude and during which the fluorescence decays is associated with an unfolding event (Figure 5c). The GdnHCl distributions of the apparent rate constants (k_{obs}) for both kinetic phases of refolding and unfolding at pH 6 are shown in Figure 5e. We note that the GdnHCl concentrations corresponding to the rate minima for the fast and slow phases are ~2.1 and ~2.5 M, respectively. Except for the unfolding by the slow kinetic phase, the rates clearly roll over as strongly nativelike and strongly unfolding conditions are approached. Classically, multiple chevrons indicate the existence of interconverting ensembles of unfolded conformations with ensemble-specific refolding rates producing parallel folding routes, and chevron rollover is thought to arise from accumulation of kinetic intermediates (*48*). For the Apaf-1 CARD, the two distinct chevrons with limb rollovers then suggest the occurrence of two ensembles of unfolded conformations, where one folds faster than the other. The two ensembles are unlikely to originate from proline cis ⇌ trans isomerization, because the rate constant for the observed slow folding−unfolding phase across the range of the denaturant concentration is much faster than the canonical rates for proline isomerization-related folding events (*49*, *50*). The folding routes for both fast folding (U_F) and slow folding (U_S) ensembles involve kinetic intermediates, but the number of intermediates involved in the folding of U_F and U_S cannot be determined with the data at hand. Available results allow the description of Apaf-1 CARD folding by the following basic model

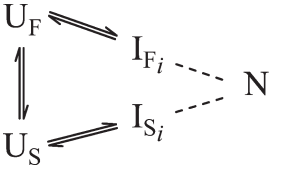

where I_{Fi} and I_{Si} represent intermediates. Except for the kinetic intermediates invoked here, this model is consistent with the one proposed earlier on the basis of the kinetic study of Apaf-1 CARD folding (*47*). That work employed urea as the denaturant unlike GdnHCl used here and observed only one chevron with no rate rollover in the limbs. Part of the discrepancy in the results may arise from the use of two different chemical denaturants. Our study provides direct evidence of distinct

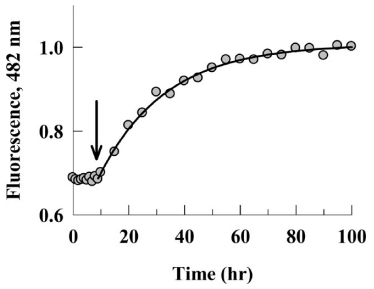

FIGURE 6: Fibrillation kinetics monitored by ThT fluorescence. The sample that contained 15 μM CARD and 50 μM ThT was held at pH 2.1 and 60 °C. The arrow indicates the end of the lag phase (~9 h). The fit of the data after the lag phase yields a k of 0.04 h^{-1}.

unfolded-state ensembles based on the finding of two distinct chevrons. Providing further details of the kinetic mechanism, including the appropriateness of the parallel folding routes depicted here, will require characterization of the $U_F \rightleftharpoons U_S$ equilibrium.

Figure 5f shows the rate−denaturant distribution for CARD folding and unfolding at pH 3.1. At all concentrations of GdnHCl, the observable fast phase in the stopped-flow kinetics is due to unfolding. This is also the case with the slow phase when the GdnHCl concentration is greater than ~0.3 M. Importantly, the GdnHCl dependences of both rates are associated with considerable positive slope or kinetic m value (given by $m_u^{\ddagger} = 2.3RT\,\partial \log k_u/\partial$[GdnHCl], where k_u is the apparent rate constant of unfolding), indicating that the CARD at pH 3.1 is still substantially structured with a defined core. Also, as it happens at pH 6, the unfolding rates at pH 3.1 roll over under strongly unfolding conditions, suggesting the occurrence of two ensembles of unfolded conformations and an unknown number of kinetic intermediates as depicted in the folding model given above. It thus appears that the structure and topology of CARD at pH 3.1 resemble those of the pre-molten globule state characterized by fluctuating structural elements (*45*).

Kinetics of Protofibril Formation for the Apaf-1 CARD. The indication provided by ANS fluorescence results (Figure 3d) that the acid-denatured and MG-like CARD can form soluble oligomers or PAs at pH ~2 led us to examine whether the precursors have the propensity to grow into protofibrils. Since the dye ThT is specifically used to probe amyloid fibrils (*51*, *52*), we incubated a 15 μM CARD solution containing 50 μM ThT at 60 °C held at pH 2.1 in Gly-HCl buffer and periodically measured the time dependence of the dye fluorescence up to 100 h. As Figure 6 shows, following a lag time of ~9 h, the fluorescence increases in a single-exponential phase with an apparent rate constant of 0.04 h^{-1}, suggesting the formation of amyloid fibrils (*53*). Generally, the presence of the lag phase and the fibrillation rate both depend on the protein concentration as well as the incubation temperature and buffer conditions used. This should hold for the formation of CARD fibrils also, although we have not explored conditions that would reduce the lag time or increase the rate of fibril formation.

Images and Dimensions of Apaf-1 CARD Fibrils. The formation of fibrils was confirmed by direct images of CARD samples held at pH 2.1 and incubated at 60 °C for varying periods of time (Figure 7). By using ~10 μM protein, we see signs of elementary combination of PA within ~15 min (Figure 7a, panel 1). The growth into protofibrils requires several hours, shown here at the end of 8 h (panel 2), and longer fibrillar structures begin to appear after incubation for ~14 h (panel 3). At ~100 μM protein, the fibrillation kinetics was very rapid (Figure 7b). The rich lattice of amyloid fibrils observed after incubation for 1 h (panel 1) becomes denser after ~3 h (panel 2) but appears diffused and dull at longer times, shown here for 9 and 20 h (panels 3 and 4, respectively).

To achieve a dimensional distinction of PA, protofibrils, and large fibrils, we determined the Gaussian distribution of diameter d for each population. The diameters measured in 116, 44, and 68 readings for PA, protofibrils, and large fibrils, respectively, were arranged into groups of 0.25 nm increments, and the percent population falling in each diameter group was determined (Figure 8). The solid lines through the data are three-parameter Gaussian fits according to

$$P(d) = P(d_o) \exp\left[-0.5\left(\frac{d-d_o}{b}\right)^2\right] \quad (1)$$

where $P(d_o)$ is the amplitude corresponding to the mean diameter d_o and b is the full width at half-maximum (fwhm). The value of d_o for PA is 2.1 nm versus 2.7 and 2.63 nm for protofibrils and elongated protofibrils, respectively. This dimensional difference between the initial PA and the fibrils should arise from differences in the content of presumably β-sheet. The fwhm values (1.5, 1.6, and 1.25 nm for the distributions corresponding to PA, protofibrils, and elongated protofibrils, respectively) indicate population inhomogeneity, being largest for protofibrils and smallest for large fibrils. The differences in the inhomogeneity may partly arise from the fact that structurally PA and fully grown fibrils are characterized by α-helical and β-sheet content, whereas the protofibrils at the initial formation stages contain both in a proportion different from one set of populations to another (large fwhm).

DISCUSSION

Examinations of the pH-induced conformational transitions and folding stability of the recombinant human Apaf-1 CARD have shown that the acid-denatured protein self-associates to form soluble precursor aggregates which can combine and undergo structural transitions to form amyloid protofibrils.

Soluble Oligomers and Protofibrils of the Apaf-1 CARD. Many pro- and antisurvival proteins of the apoptotic machinery are known to homodimerize, heterodimerize, and even homo-oligomerize to exert their survival and death effects (*54*−*62*). Some are constitutively oligomeric because of the ready accessibility of the interacting surfaces, and others are prevented from oligomerization by sequestration of the interacting surfaces until functional activation occurs. The former class is exemplified by the prosurvival protein Bcl-x_L, for which a large fraction of the cellular population homodimerizes by homophilic interaction of the C-terminal hydrophobic tails (*44*, *62*−*64*), and the latter is represented by quiescent Apaf-1 known to exist in the monomeric form (*36*, *65*). It appears that the structural surface of the CARD of Apaf-1 required for homophilic interaction with the CARD of procaspase-9 (*38*) is partially buried in the inactive state of Apaf-1 due to intramolecular interactions, an observation based on the crystal structure of WD40-deleted Apaf-1 (*66*). When activated by binding with cytochrome c and dATP (*65*), Apaf-1 forms a wheel-shaped homoheptamer complex or apoptosome having 7-fold symmetry (*67*, *68*). Although atomic details and packing interactions for the apoptosome are not known, the CARD can now interact with the CARD of procaspase-9. Thus, homoheptamerization of Apaf-1 seems to be crucial for sensitizing the CARD for binding interactions.

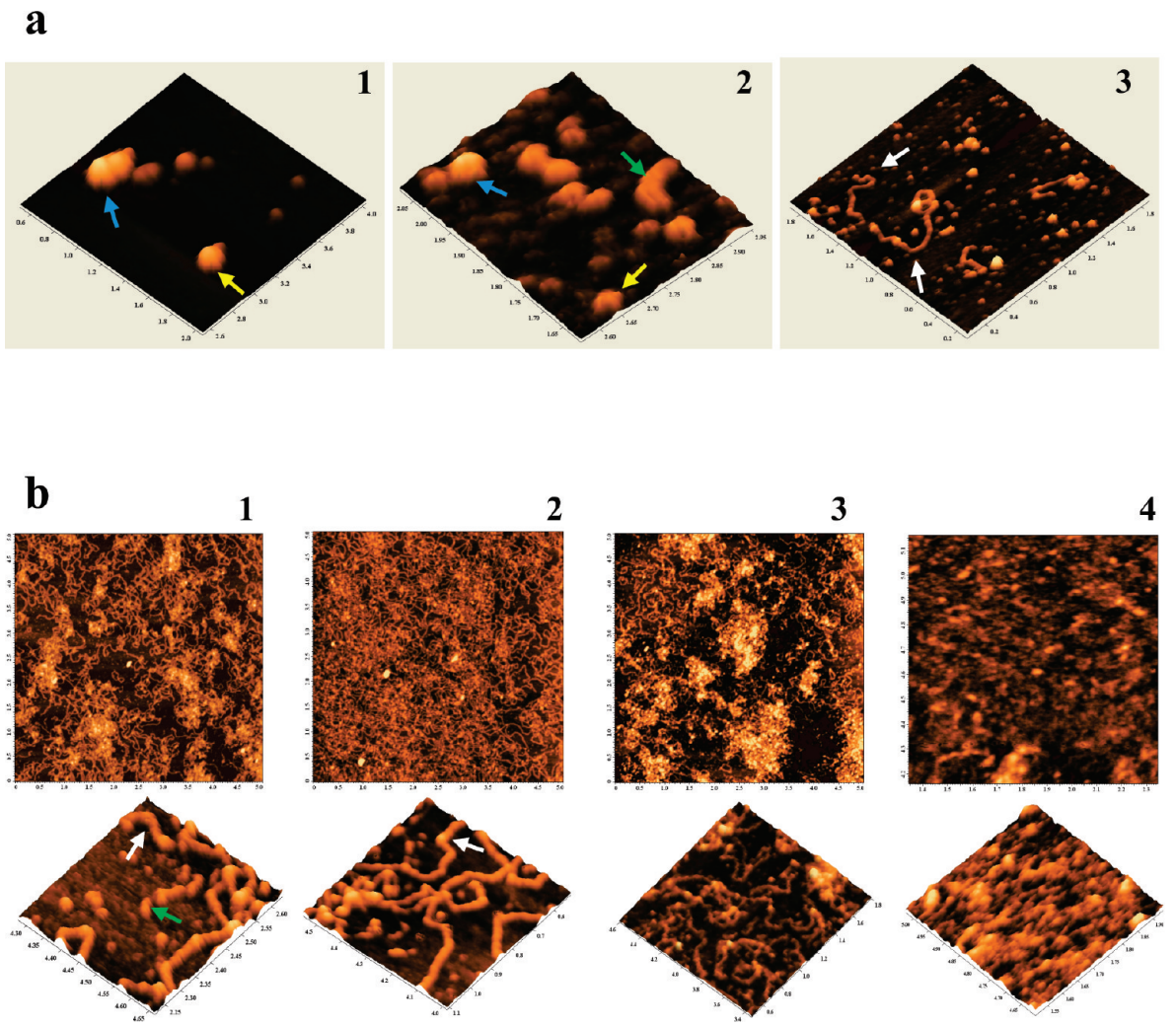

FIGURE 7: AFM images of Apaf-1 CARD aggregates. (a) A 10 μM protein solution incubated at 60 °C and pH 2.1 shows the first signs of combination of the PA within ~15 min (panel 1). The growth and elongation of protofibrils are shown in panels 2 and 3 imaged after incubation for 8 and 14 h, respectively. Yellow, blue, green, and white arrows denote PA, elongated PA, nascent protofibrils, and elongated protofibrils, respectively. (b) At ~100 μM protein, fast and rich growth of fibrils is observed. Imgaes shown in panels 1−4 were recorded with samples incubated for 1, 3, 9, and 20 h, respectively. An enlarged view of a small area is shown below each panel.

However, the Apaf-1 CARD alone in neutral-pH solutions exists in the monomeric state (Figures 3−5), consistent with the earlier report that no dimerization occurs even at concentrations as high as 1 mM (*38*). On the other hand, the isolated Apaf-1 CARD forms a complex with the isolated caspase-9 CARD in which the former deploys sets of acidic and hydrophobic residues in a manner that creates a contiguous binding surface, suggesting that intermolecular associations of the Apaf-1 CARD require both electrostatic and hydrophobic interactions (*38*). Should the Apaf-1 CARD alone undergo homo-oligomerization, the operative forces of interaction must be hydrophobic in nature, because surface charge complementarity is not available. The existence of the Apaf-1 CARD in the monomeric form in the neutral-pH region suggests that the hydrophobic interactions afforded by the native protein surface are insufficient for dimerization to occur. The situation is quite interesting under acidic conditions (pH ~3−4) where the CARD undergoes a MG-like transition. Relative to that in the native state, the molecular surface in the MG state is more hydrophobic as evidenced by binding of small nonpolar molecules like ANS (Figure 3b,c). The increased surface hydrophobicity should favor CARD−CARD self-association, but electrostatic repulsion due to excess positive charge and large-scale fluctuations of the structural elements in the MG-like state (*45*) are the principal opposing forces. A dramatic increase in surface hydrophobicity can occur under strongly acidic conditions (pH <2.5) where the already weakened structural elements of the CARD MG break down, causing exposure of buried nonpolar residues. We believe the preponderance of hydrophobic surfaces in the acid-denatured proteins is now so overwhelmingly favorable toward CARD oligomerization that electrostatic repulsions are subdued, and a monomer ⇌ oligomer equilibrium is readily established. The oligomerization event can be considered a transition to an alternative non-native global free energy minimum (*69*). We should also note that protein oligomerization by hydrophobic interactions at low pH very likely buries some positive charges in the protein−protein apolar interface, and because charge burial in the low-dielectric apolar environment is energetically expensive, the CARD oligomers are unlikely to be very highly stable.

These soluble oligomers are precursor aggregates (PAs) which grow in size to form elongated protofibrils (PA → protofibril). We have not investigated the mechanism and the events associated with the PA → protofibril condensation in this work, but the CARD fibrillation pathway may be depicted as

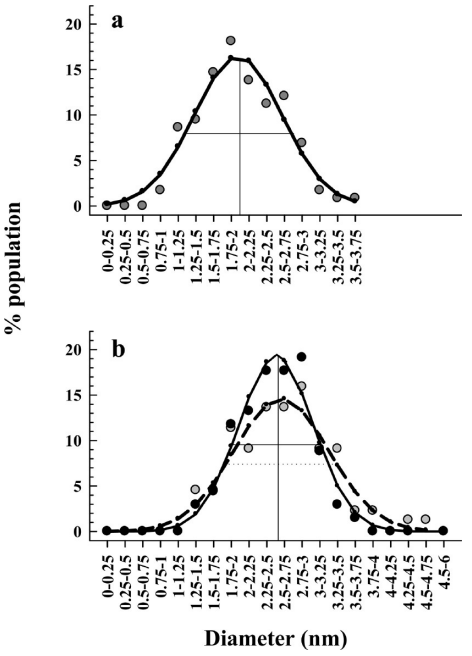

FIGURE 8: Distribution of population diameters. The solid lines are three-parameter Gaussian fits to the measured data according to eq 1. (a) PA with a mean diameter d_o of 2.1 nm. (b) Protofibrils and elongated protofibrils with d_o values of 2.7 and 2.63 nm, respectively.

MG ⇋ PA → protofibril → elongated protofibril. The inference that the MG-like conformation facilitates PA formation is consistent with the survey-based study which showed that the amyloidogenic conformation shares many structural and dynamic properties with the pre-molten globule state (*2*).

Relevance to in Vivo Fibrillation of Apaf-1?. Although we obtained amyloid fibrils from the acid-denatured CARD at an elevated temperature, the question is the relevance this has for in vivo situations, given that none of the pro- and antisurvival proteins is known to undergo fibrillation. This study rests on a limited empirical search for an in vitro condition that facilitates fibrillation. The low pH and high temperature encourage higher surface hydrophobicity for the monomers and stronger hydrophobic interactions between them, respectively. Such conditions are certainly not physiological, but one cannot exclude yet unknown intrinsic cellular factors, accidental biochemical insults, or pathological conditions that could promote formation of soluble oligomers of Apaf-1 required for protofibril growth. As mentioned earlier, fibril growth may require some combination of the initial molecular structure, packing density, bonding, intramolecular dynamics, and surface dielectric (*5*, *8*−*13*). Since the underlying physicochemical principles of fibril growth are not fully understood, the conditions that might promote fibrillation in vivo need to be empirically determined. Facing the two counteracting scenarios (the absence of specific evidence for amyloidosis of apoptotic proteins on one hand and the finding that the CARD could undergo fibrillation, albeit under nonphysiological conditions, on the other), one could at the most say that there is a very low or a restricted likelihood of Apaf-1 fibrillation in vivo. Even this likelihood could be narrowed for a protein the size of Apaf-1 given that amyloidogenic proteins and peptides are generally smaller. The CARD is a small domain of Apaf-1, and it independently might not form fibrillar aggregates under physiological conditions. Thus, in vivo fibrillation of Apaf-1 appears highly unlikely.

Amyloid Fibrils, Cytotoxicity, and Apoptosis. The cytotoxicity of amyloid fibrils and progression of degenerative disorders such as Alzheimer's and Creutzfeldt-Jacob diseases due to insoluble fibrils of amyloid-β protein (Aβ) and prion protein (PrP), respectively (*31*−*35*, *70*, *71*), are well-established. It is also recognized that activation of an apoptotic pathway is one of the major causes of amyloid fibril-induced cell death (*27*−*30*), but the issue of cytotoxicity of prefibrillar aggregates of pro- and antisurvival apoptotic proteins, even if one or more of them could undergo in vivo fibrillation, is redundant. Cytotoxicity is irrelevant here because prefibrillar aggregates of any of these proteins as such would be very detrimental to cell survival. Since Apaf-1 is the key antisurvival protein of the mitochondrial pathway of apoptosis in neuronal and non-neuronal cells alike, amyloid fibrillation of this protein will arrest normal development of organs in adults and lack of embryonic differentiation leading to death, just the way Apaf-1-null mice die due to a pronounced enlargement of the periventricular proliferative zone during late embryonic development (*72*).

ACKNOWLEDGMENT

We thank Rajeshwar S. Sankhala for help with AFM imaging.

REFERENCES

1. Hardy, J., and Selkoe, D. J. (2002) The amyloid hypothesis of Alzheimer's disease: Progress and problems on the road to therapeutics. *Science 297*, 353–356.
2. Uversky, V. N., and Fink, A. L. (2004) Conformational constraints for amyloid fibrillation: The importance of being unfolded. *Biochim. Biophys. Acta 1698*, 131–153.
3. Perry, G., Cras, P., Siedlak, S. L., Tabaton, M., and Kawai, M. (1992) Beta protein immunoreactivity is found in the majority of neurofibrillary tangles of Alzheimer's disease. *Am. J. Pathol. 140*, 283–290.
4. Selkoe, D. J. (1991) The molecular pathology of Alzheimer's disease. *Neuron 6*, 487–498.
5. Chiti, F., and Dobson, C. M. (2006) Protein misfolding, functional amyloid, and human disease. *Annu. Rev. Biochem. 75*, 333–366.
6. Selkoe, D. (2003) Folding proteins in fatal ways. *Nature 426*, 900–904.
7. Soto, C., Estrada, L., and Castilla, J. (2006) Amyloids, prions and the inherent infectious nature of misfolded protein aggregates. *Trends Biochem. Sci. 31*, 150–155.
8. Stefani, M., and Dobson, C. M. (2003) Protein aggregation, and aggregate toxicity: New insights into protein folding, misfolding diseases and biological evolution. *J. Mol. Med. 81*, 678–699.
9. Makin, O. S., Atkins, E., Sikorski, P., Johansson, J., and Serpell, L. C. (2005) Molecular basis for amyloid fibril formation and stability. *Proc. Natl. Acad. Sci. U.S.A. 102*, 315–320.
10. Dobson, C. M. (2003) Protein folding and misfolding. *Nature 426*, 884–890.
11. Lee, Y.-H., Chatani, E., Sasahara, K., Naiki, H., and Goto, Y. (2009) A comprehensive model for packing and hydration for amyloid fibrils of β_2-microglobulin. *J. Biol. Chem. 284*, 2169–2175.
12. Bucciantini, M., Giannoni, E., Chiti, F., Baroni, F., Formigli, L., Zurdo, J., Taddei, N., Ramponi, G., Dobson, C. M., and Stefani, M. (2002) Inherent toxicity of aggregates implies a common mechanism for protein misfolding diseases. *Nature 416*, 507–511.
13. Mishra, P., and Bhakuni, V. (2009) Self-assembly of bacteriophage-associated hyaluronate lyase (HYLP2) into an enzymatically active fibrillar film. *J. Biol. Chem. 284*, 5240–5249.
14. Vendruscolo, M., Zurdo, J., MacPhee, C. E., and Dobson, C. M. (2003) Protein folding and misfolding: A paradigm of self-assembly and regulation in complex biological systems. *Philos. Trans. R. Soc. London, Ser. A 361*, 1205–1222.
15. Fändrich, M. V., Forge, V., Buder, K., Kittler, M., Dobson, C. M., and Diekmann, S. (2003) Myoglobin forms amyloid fibrils by association of unfolded polypeptide segments. *Proc. Natl. Acad. Sci. U.S.A. 100*, 15463–15468.
16. Juarez, J., Taboada, P., and Mosquera, V. (2009) Existence of different structural intermediates on the fibrillation pathway of human serum albumin. *Biophys. J. 96*, 2353–2370.
17. Makin, O. S., and Serpell, L. C. (2005) Structures for amyloid fibrils. *FEBS J. 272*, 5950–5961.
18. Nelson, R., and Eisenberg, D. (2006) Structural models of amyloid-like fibrils. *Adv. Protein Chem. 73*, 235–282.

19. Nelson, R., and Eisenberg, D. (2006) Recent atomic models of amyloid fibril structure. *Curr. Opin. Struct. Biol. 16*, 260–265.
20. Walsh, P., Simonetti, K., and Sharpe, S. (2009) Core structure of amyloid fibrils formed by residues 106−126 of the human prion protein. *Structure 17*, 417–426.
21. Zhang, S. (2003) Fabrication of novel biomaterials through molecular self-assembly. *Nat. Biotechnol. 21*, 1171–1178.
22. Ryadnov, M. G., and Woolfson, D. M. (2003) Engineering the morphology of a self-assembling protein fibre. *Nat. Mater. 2*, 329–332.
23. Reches, M., and Gazit, E. (2003) Casting metal nanowires within discrete self-assembled peptide nanotubes. *Science 300*, 625–627.
24. Rajagopal, K., and Schneider, J. P. (2004) Self-assembling peptides and proteins for nanotechnological applications. *Curr. Opin. Struct. Biol. 14*, 480–486.
25. Gazit, E. (2007) Use of biomolecular templates for the fabrication of metal nanowires. *FEBS J. 274*, 317–322.
26. Hamley, I. W. (2007) Peptide fibrillization. *Angew. Chem., Int. Ed. 46*, 8128–8147.
27. Loo, D. T., Copani, A., Pike, C. J., Whittemore, E. R., Walencewicz, A. J., and Cotman, C. W. (1993) Apoptosis is induced by β-amyloid in cultured central nervous system neurons. *Proc. Natl. Acad. Sci. U.S. A. 90*, 7951–7955.
28. Yuan, J., and Yankner, B. A. (2000) Apoptosis in the nervous system. *Nature 407*, 802–809.
29. Zhang, Y., McLaughlin, R., Goodyer, C., and LeBlanc, A. (2002) Selective cytotoxicity of intracellular amyloid β peptide$_{1-42}$ through p53 and Bax in cultured primary human neurons. *J. Cell Biol. 156*, 519–529.
30. Novitskaya, V., Bocharova, O. V., Bronstein, I., and Baskakov, I. V. (2006) Amyloid fibrils of mammalian prion protein are highly toxic to cultured cells and primary neurons. *J. Biol. Chem. 281*, 13828–13836.
31. Forloni, G., Angeretti, N., Chiesa, R., Monzani, E., Salmona, M., Bugiani, O., and Tagliavini, F. (1993) Neurotoxicity of a prion protein fragment. *Nature 362*, 543–536.
32. Giese, A., Brown, D. R., Groschup, M. H., Feldmann, C., Haist, I., and Kretzschmar, H. A. (1998) Role of microglia in neuronal cell death in prion disease. *Brain Pathol. 8*, 449–457.
33. Brown, D. R., Schmidt, B., and Kretzschmar, H. A. (1996) Role of microglia and host prion protein in neurotoxicity of a prion protein fragment. *Nature 380*, 345–347.
34. Hetz, C., Russelakis-Carneiro, M., Maundrell, K., Castilla, J., and Soto, C. (2003) Caspase-12 and endoplasmic reticulum stress mediate neurotoxicity of pathological prion protein. *EMBO J. 22*, 5435–5445.
35. Gu, Y., Fujioka, H., Mishra, R. S., Li, R., and Singh, N. (2002) Prion Peptide 106−126 Modulates the Aggregation of Cellular Prion Protein and Induces the Synthesis of Potentially Neurotoxic Transmembrane PrP. *J. Biol. Chem. 277*, 2275–2286.
36. Zou, H., Li, Y., Liu, X., and Wang, X. (1999) An Apaf-1·cytochrome *c* multimeric complex is a functional apoptosome that activates procaspase-9. *J. Biol. Chem. 274*, 11549–11556.
37. Hu, Y., Benedict, M. A., Ding, L., and Núñez, G. (1999) Role of cytochrome *c* and dATP/ATP hydrolysis in Apaf-1-mediated caspase-9 activation and apoptosis. *EMBO J. 18*, 3586–3595.
38. Zhou, P., Chou, J., Olea, R. S., Yuan, J., and Wagner, G. (1999) Solution structure of Apaf-1 CARD and its interaction with caspase-9 CARD: A structural basis for specific adaptor/caspase interaction. *Proc. Natl. Acad. Sci. U.S.A. 96*, 11265–11270.
39. Yan, N., and Shi, Y. (2005) Mechansims of apoptosis through structural biology. *Annu. Rev. Cell Dev. Biol. 21*, 35–56.
40. Chou, J. J., Matsuo, H., Duan, H., and Wagner, G. (1998) Solution structure of the RAIDD CARD and model for CARD/CARD interaction in caspase-2 and caspase-9 recruitment. *Cell 94*, 171–180.
41. Liang, H., and Fesik, S. W. (1997) Three-dimensional structures of proteins involved in programmed cell death. *J. Mol. Biol. 274*, 291–302.
42. Nagato, S. (1997) Apoptosis by death factor. *Cell 88*, 355–365.
43. Qin, H., Srinivasula, S. M., Wu, G., Fernandes-Alnemri, T., Alnemri, E. S., and Shi, Y. (1999) Structural basis of procaspase-9 recruitment by the apoptotic protease-activating factor 1. *Nature 399*, 549–557.
44. Xie, Z., Schendel, S., Matsuyama, S., and Reed, J. C. (1998) Acidic pH promotes dimerization of Bcl-2 family proteins. *Biochemistry 37*, 6410–6418.
45. Ptitsyn, O. B. (1995) Molten globule and protein folding. *Adv. Protein Chem. 47*, 83–229.
46. Santoro, M. M., and Bolen, D. W. (1988) Unfolding free energy changes determined by the linear extrapolation method. 1. Unfolding of phenylmethanesulfonyl α-chymotrypsin using different denaturants. *Biochemistry 27*, 8063–8068.
47. Milam, S. L., Nicely, N. I., Feeney, B., Mattos, C., and Clark, A. C. (2007) Rapid folding and unfolding of Apaf-1 CARD. *J. Mol. Biol. 369*, 290–304.
48. Matouschek, A., Kellis, J. T., Serrano, L., Bycroft, M., and Fersht, A. R. (1990) Transient folding intermediates characterized by protein engineering. *Nature 346*, 440–445.
49. Sakata, M., Chatani, E., Kameda, A., Sakurai, K., Naiki, H., and Goto, Y. (2008) Kinetic coupling of folding and prolyl isomerization of β_2-microglobulin studied by mutational analysis. *J. Mol. Biol. 302*, 1242–1255.
50. Jakob, R. P., and Schmid, F. X. (2009) Molecular determinants of a native-state prolyl isomerization. *J. Mol. Biol. 387*, 1017–1031.
51. LeVine, H. (1995) Thioflavin T interaction with amyloid β-sheets structure. *Amyloid 2*, 1–6.
52. Naiki, H., Higuchi, K., Hosokawa, M., and Takeda, T. (1989) Fluorometric determination of amyloid fibrils in vitro using the fluorescent dye, Thioflavin T. *Anal. Biochem. 177*, 244–249.
53. Munishkina, L. A., and Fink, A. L. (2007) Fluorescence as a method to reveal structures and membrane-interactions of amyloidogenic proteins. *Biochim. Biophys. Acta 1768*, 1862–1885.
54. O'Neill, J. W., Manion, M. K., Maguire, B., and Hockenbery, D. M. (2006) Bcl-xL dimerization by three-dimensional domain swapping. *J. Mol. Biol. 356*, 367–381.
55. Reed, J. C. (1994) Bcl-2 and the regulation of programmed cell death. *J. Cell Biol. 124*, 1–6.
56. Wei, M. C., Zong, W. Z., Cheng, E. H. Y., Lindsten, T., Panoutsakapoulou, V., Ross, A. J., Roth, K. A., MacGregor, G. R., Thompson, C. B., and Korsmeyer, S. J. (2001) Proapoptotic Bax and Bak: A requisite gateway to mitochondrial dysfunction and death. *Science 292*, 727–730.
57. Kelekar, A., Chang, B. S., Harlan, J. E., Fesik, S. W., and Thompson, C. B. (1997) Bad is a BH3 domain-containing protein that forms an inactivating dimmer with Bcl-x_L. *Mol. Cell. Biol. 17*, 7040–7046.
58. Eskes, R., Desagher, S., Antonsson, B., and Martinou, J. C. (2000) Bid induces the oligomerization and insertion of Bax into the outer mitochondrial membrane. *Mol. Cell. Biol. 20*, 929–935.
59. Wei, M. C., Lindsten, T., Mootha, V. K., Weiler, S., Gross, A., Ashiya, M., Thompson, C. B., and Korsmeyer, S. J. (2000) tBid, a membrane targeted death ligand, oligomerizes Bak to release cytochrome *c*. *Genes Dev. 14*, 2060–2071.
60. Cheng, E. H., Wei, M. C., Weiler, S., Flavell, R. A., Mak, T. W., Lindsten, T., and Korsmeyer, S. J. (2001) Bcl-x_L sequester BH3 domain-only molecules preventing Bax- and Bak mediated mitochondrial apoptosis. *Mol. Cell 8*, 705–711.
61. Ruffolo, S. C., and Shore, G. C. (2003) Bcl-2 selectively interacts with the Bid-induced open conformer of Bak, inhibiting Bak auto-oligomerization. *J. Biol. Chem. 278*, 25039–25045.
62. Yadaiah, M., Nageswara Rao, P., Harish, P., and Bhuyan, A. K. (2007) High affinity binding of Bcl-x_L to cytochrome *c*: Implication for a possible interception of translocated cytochrome *c* in apoptosis. *Biochim. Biophys. Acta 1774*, 1370–1379.
63. Antonsson, B., Montessuit, S., Sanchez, B., and Martinou, J. C. (2001) Bax is present as a high molecular weight oligomer/complex in the mitochondrial membrane of apoptotic cells. *J. Biol. Chem. 276*, 11615–11623.
64. Basanez, G., Zhang, J., Chau, B. N., Maksaev, G. I., Frolov, V. A., Brandt, T. A., Burch, J., Hardwick, J. M., and Zimmerberg, J. (2004) Pro-apoptotic cleavage products of Bcl-x_L form cytochrome *c*-conducting pores in pure lipid membranes. *J. Biol. Chem. 276*, 31083–31091.
65. Li, P., Nijhawan, D., Budihardjo, I., Srinivasula, S. M., Ahmad, M., Alnemri, E. S., and Wang, X. (1997) Cytochrome c and dATP-dependent formation of Apaf-1/caspase-9 complex initiates an apoptotic protease cascade. *Cell 91*, 479–489.
66. Riedl, S. J., Li, W., Schwarzenbacher, R., and Shi, Y. (2005) Structure of the apoptotic protease-activating factor 1 bound to ADP. *Nature 434*, 926–933.
67. Acehan, D., Jiang, X., Morgan, D. G., Heuser, J. E., Wang, X., and Akey, C. W. (2002) Three dimensional structure of the apoptosome: Implications for assembly, procaspase-9 binding and activation. *Mol. Cell 9*, 423–432.
68. Yu, X., Acehan, D., Ménétret, J., Booth, C. R., Ludtke, S. J., Riedl, S. J., Shi, Y., Wang, X., and Akey, C. W. (2005) A structure of the human apoptosome at 12.8 Å resolution provides insights into this cell death platform. *Structure 13*, 1725–1735.
69. Gazit, E. (2002) The "correctly folded" state of proteins: Is it a metastable state?. *Angew. Chem., Int. Ed. 41*, 257–259.
70. Yankner, B. A. (1996) Mechanisms of neuronal degeneration in Alzheimer's disease. *Neuron 16*, 921–932.
71. Guela, C., Wu, C.-K., Saroff, D., Lorenzo, A., Yuan, M., and Yankner, B. A. (1998) Aging renders the brain vulnerable to amyloid β-protein neurotoxicity. *Nat. Med. 4*, 827–831.
72. Cecconi, F., Alvarez-Bolado, G., Meyer, B. I., Roth, K. A., and Gruss, P. (1998) Apaf1 (CED-4 homolog) regulates programmed cell death in mammalian development. *Cell 94*, 727–737.